Report

Current Biology

Responses to Spatial Contrast in the Mouse Suprachiasmatic Nuclei

Highlights

- Many SCN units have receptive fields optimized for spatial discrimination
- A large majority of SCN neurons track changes in spatial patterns
- Spatial patterns can enhance SCN-maintained firing, but not circadian phase resetting

Authors

Joshua W. Mouland, Adam R. Stinchcombe, Daniel B. Forger, Timothy M. Brown, Robert J. Lucas

Correspondence

robert.lucas@manchester.ac.uk

In Brief

Mouland et al. show that neurons in the SCN are optimized for spatial resolution and are responsive to visual patterns. This greatly extends the range of visual stimuli that could influence autonomic and vegetative systems under the SCN's control.

Mouland et al., 2017, Current Biology *27*, 1633–1640
June 5, 2017
http://dx.doi.org/10.1016/j.cub.2017.04.039

CellPress

Current Biology
Report

Responses to Spatial Contrast in the Mouse Suprachiasmatic Nuclei

Joshua W. Mouland,[1] Adam R. Stinchcombe,[2] Daniel B. Forger,[2,3] Timothy M. Brown,[1] and Robert J. Lucas[1,4,*]
[1]Faculty of Biology, Medicine and Health, University of Manchester, Manchester M13 9PT, UK
[2]Department of Mathematics, University of Michigan, 2074 East Hall, 530 Church Street, Ann Arbor, MI 48109-1043, USA
[3]Department of Computational Medicine and Bioinformatics, University of Michigan, Ann Arbor, MI 48109, USA
[4]Lead Contact
*Correspondence: robert.lucas@manchester.ac.uk
http://dx.doi.org/10.1016/j.cub.2017.04.039

SUMMARY

A direct retinal projection targets the suprachiasmatic nucleus (SCN) (an important hypothalamic control center). The accepted function of this projection is to convey information about ambient light (irradiance) to synchronize the SCN's endogenous circadian clock with local time and drive the diurnal variations in physiology and behavior [1–4]. Here, we report that it also renders the SCN responsive to visual images. We map spatial receptive fields (RFs) for SCN neurons and find that only a minority are excited (or inhibited) by light from across the scene as expected for irradiance detectors. The most commonly encountered units have RFs with small excitatory centers, combined with very extensive inhibitory surrounds that reduce their sensitivity to global changes in light in favor of responses to spatial patterns. Other units have larger excitatory RF centers, but these always cover a coherent region of visual space, implying visuotopic order at the single-unit level. Approximately 75% of light-responsive SCN units modulate their firing according to simple spatial patterns (drifting or inverting gratings) without changes in irradiance. The time-averaged firing rate of the SCN is modestly increased under these conditions, but including spatial contrast did not significantly alter the circadian phase resetting efficiency of light. Our data indicate that the SCN contains information about irradiance and spatial patterns. This newly appreciated sensory capacity provides a mechanism by which behavioral and physiological systems downstream of the SCN could respond to visual images [5].

RESULTS

Spatial Receptive Fields in the SCN

Measuring irradiance, by definition, is achieved by integrating incident light from across the visual scene. In non-mammalian vertebrates, this task is readily achieved by having the photoreceptor cells responsible for entraining circadian clocks in tissues (e.g., pineal gland, deep brain, and peripheral tissues) that lack the optical apparatus to render them differentially sensitive to light from different parts of visual space [6]. However, entrainment in mammals originates in the eye, an organ specifically designed to retain information about spatial patterns. As a result, the individual photoreceptors (rods, cones, and intrinsically photosensitive retinal ganglion cells [ipRGCs]) responsible for entraining the clock are each responsive to light from a limited portion of visual space [7]. This raises the question of how the suprachiasmatic nucleus (SCN) deals with the spatial information produced by this arrangement. One possibility is that it is discarded, with SCN connectivity and/or the retinal projection arranged in such a way as to render individual SCN neurons responsive to light from across the visual scene. This would allow each neuron to act as a perfect irradiance detector. In the only published exploration of this aspect of SCN physiology, Groos and Mason [8] measured spatial receptive fields (RFs) for a small number of units in the cat. Their data provide partial support for this hypothesis, with RFs extended over large areas of visual space (consistent with the expectation of substantial spatial integration), but not across the whole scene (as expected for perfect irradiance detectors). The conclusion that spatial integration is imperfectly achieved is supported by the more recent observation that few units in the mouse SCN show binocular sensitivity [9].

Here, we set out to determine more exactly the extent to which individual SCN neurons are capable of integrating light input irrespective of its spatial location and how electrophysiological activity and the circadian entrainment mechanism are impacted by spatial contrast. We started by mapping spatial receptive fields for SCN neurons. Multichannel extracellular recording electrodes were introduced into the SCN of anesthetized mice and a display covering 70° by 110° of visual space used to present horizontal or vertical white bars (6°–8° width) against a dark background. Bars were presented at high temporal frequency (duration = 250 ms; inter-stimulus interval = 250 ms) to maximize the number of stimulus repeats while strongly biasing responses in favor of rod/cone versus melanopsin origin ([10, 11]; see also [12] in this issue). Multiunit activity was spike sorted to record the activity of 27 individual light-responsive units sampled from 11 mice (Figure S1) and their response to bar stimuli defined by the probability of firing per unit time (presented as a firing rate). We found both examples of units whose firing rate was either increased or decreased by the appearance of bars (Figure 1).

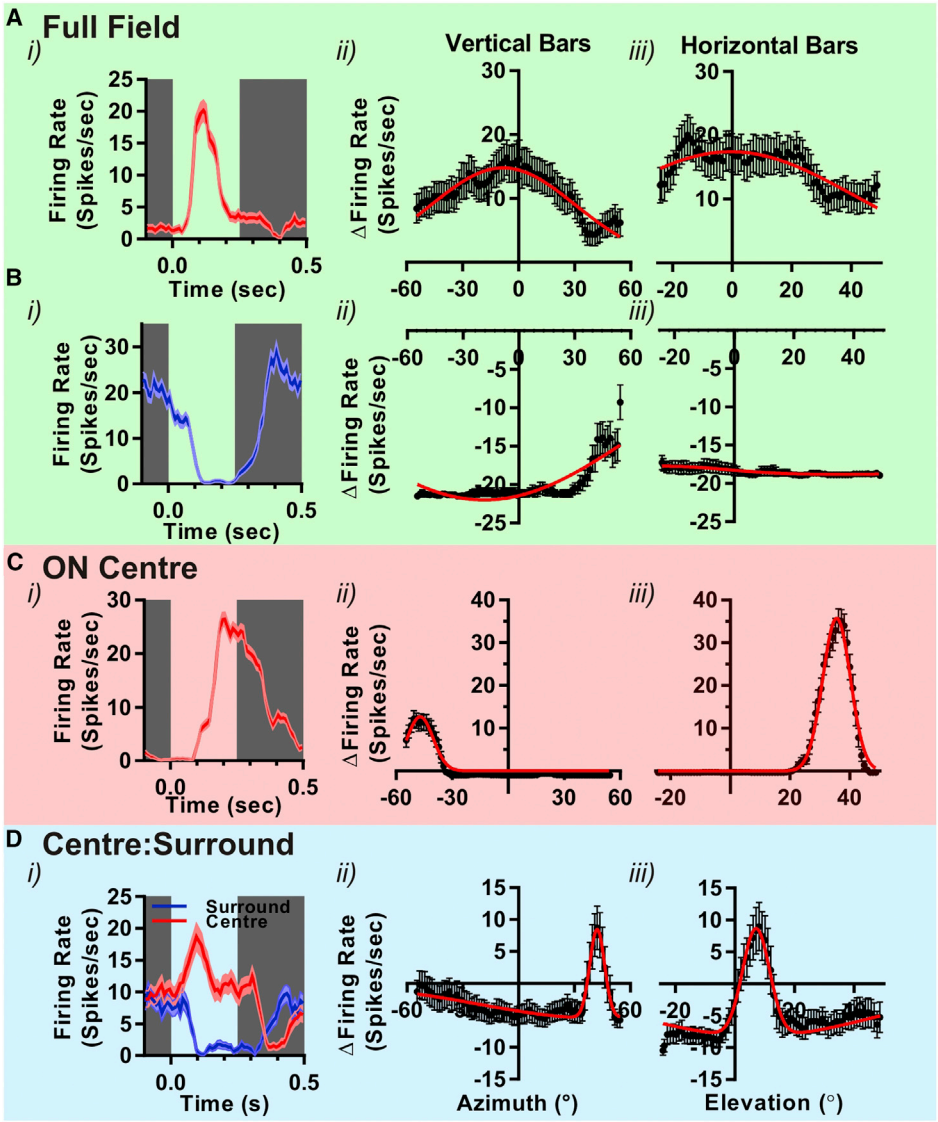

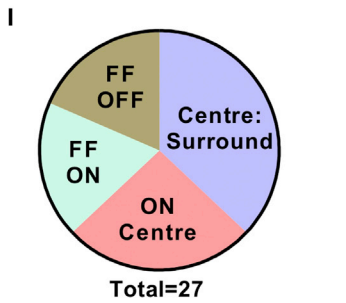

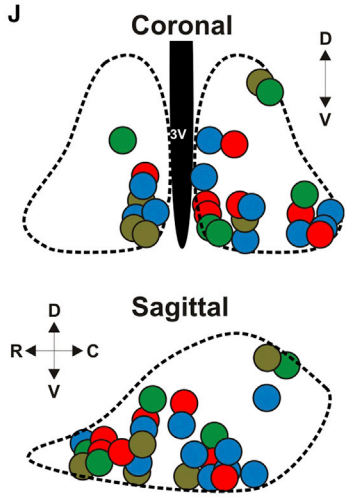

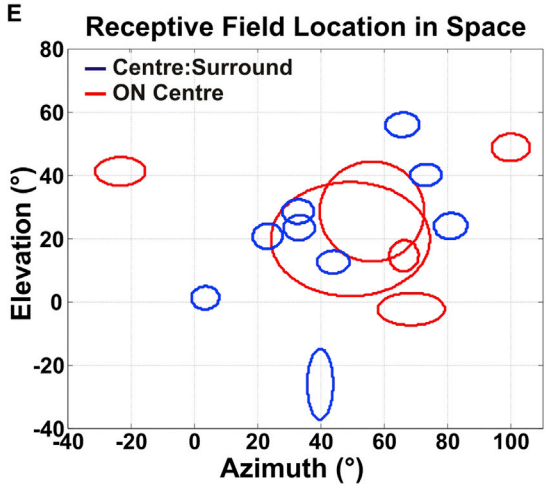

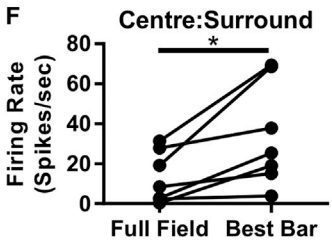

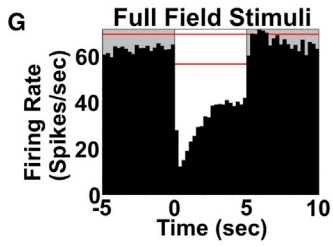

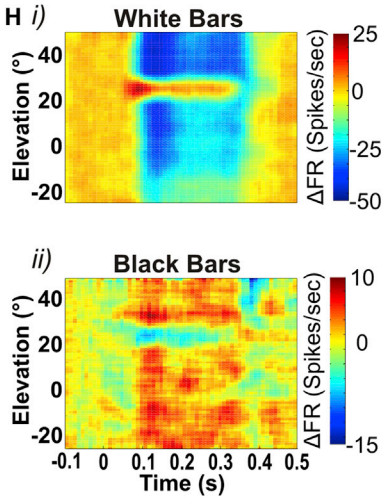

(legend on next page)

If individual SCN units were irradiance detectors, we would expect them to be excited by bars wherever they appeared in visual space. Five of 27 units displayed such behavior (Figure 1A; hereinafter termed "full field ON" units), showing increases in firing following the appearance of white bars whether in horizontal or vertical orientation and across the full extent of the display. Another group of units ("full field OFF" units; n = 5) responded to bars in all positions but this time with a reduction in firing (Figure 1B).

The response of the remaining units (17/27) was strongly dependent upon bar location (Figures 1C and 1D). Seven of these had a spatially constrained excitatory center ("ON center" units; Figure 1C), over which bars increased firing, but were refractory to the appearance of bars over the rest of the visual scene. RF centers for this population varied substantially in diameter from ~10° to >40° (Figure 1E). As RFs for the M1 class of ipRGC that dominate the retinohypothalamic tract [13] are around 10° in mice (based upon dendritic field size [14] and the structural physiology of the mouse eye [15]), this implies that, in many cases, SCN neurons received excitatory input from numerous retinal ganglion cells.

The remaining (10/27) were excited by bars over a small region of visual space (Figure 1D) but inhibited by bars elsewhere in the visual scene. Thus, these "center:surround" units had RFs comprising of an excitatory ON center and an inhibitory OFF surround. ON centers were approximately circular and ranged from 8° to 16° in diameter (Figure 1E), implying excitatory input from a single retinal ganglion cell in most cases. The inhibitory surround extended across the remainder of the screen. In a subset of recordings, we shifted the location of the screen by 30° in an attempt to define the limits of the OFF surround. We found inhibitory responses also at this new location (data not shown), indicating that OFF surrounds encompass very large portions of visual space.

The most commonly encountered RF type was thus center:surround (Figure 1I). Moreover, our method probably underestimates their occurrence, as the distinction between this group and full field OFF or "ON center" units relies upon negative data (failure to observe excitatory or inhibitory responses, respectively; see STAR Methods). There was no strong bias in either the anatomical location of units with the various RF types within the SCN (Figure 1J) or the location of their RFs in visual space (Figure 1E). ON centers were significantly smaller in center:surround than in ON center units (n = 10 center:surround and 6 ON center units mappable in both dimensions; mean ± SEM = 9.7° ± 0.7° and 18.6° ± 5.2°, respectively; t test; $p = 0.03$).

The appearance of center:surround antagonism implies that diffuse increases in irradiance are not the favored visual stimulus for many SCN neurons. To test this prediction, we compared responses of these neurons to bars in the center of their receptive field and to a full-field stimulus of equivalent radiance (but much larger irradiance). We found that, indeed, firing rates were significantly enhanced when presented with the preferred bar compared to the full-field stimulus (Figure 1F; paired t test; $p < 0.05$). In the extreme, this effect was large enough to switch the polarity of the light response from excitatory, for a bar encompassing the RF center, to inhibitory for a full-field stimulus (Figure 1G). Inhibitory responses to full-field stimuli have been previously observed in the SCN [1, 3, 4, 16] but are not encountered in afferent ipRGCs. These data reveal how they could be a product of the unexpected spatial preference of SCN neurons. Another implication of our data is that center:surround units should be excited by light decrements over much of the scene. We tested this prediction for a subset of units by presenting dark bars against a white screen and found that this was indeed the case (Figure 1H).

Response to Spatial Patterns

A clear majority of SCN units thus showed spatial preference in their visual response. There is a strong expectation that such units should respond to changes in the spatial distribution of light even in the absence of a change in global light intensity (irradiance). To test this prediction, we recorded extracellular activity in the SCN of anesthetized mice presented with inverting (~4 and 2 Hz) vertical gratings (1:600 contrast ratio 0.017–1 cycles per degree [cpd]; Figure 2A). Of 24 light-responsive single units recorded from six mice, 20 showed a significant modulation in firing rate associated with one or more of the gratings tested (see STAR Methods). The likelihood of observing a significant modulation for each unit and across the population was inversely related to spatial frequency (Figures 2A and 2B).

As predicted, a large fraction of neurons (14/16) with spatially constrained receptive fields (center:surround or ON center) tracked grating inversions at one or more of the spatial

Figure 1. Spatial Receptive Fields in the Mouse SCN

(A–D) Responses to the receptive field mapping protocol of single units representative of full-field ON (A), full-field OFF (B), ON center (C), and center:surround (D) response types. In each case, the panel to left (i) shows modulation in firing rate (10-ms bins with a five-bin boxcar average; mean ± SEM) associated with the appearance of a white bar between time 0 and 0.25 s at the location eliciting maximum response (or for center:surround maximum excitation [red] and inhibition [blue]); the center and right panels are the mean ± SEM change firing from baseline (relative to preceding 100 ms) following appearance of vertical (ii) or horizontal (iii) bars as a function of location on azimuth or elevation of bar center (0° corresponds to point directly in front of center of eye). Red lines depict difference of Gaussian fit.

(E) Projection of RFs for ON center (red) and center:surround (blue) responses in visual space (0° corresponds to point directly in front of center of eye).

(F) Comparison of firing rates for ten center:surround units under full white screen (full field) or a white bar at preferred spatial location ("best bar"; paired t test; $p < 0.05$).

(G) Change in mean firing rate (250-ms bins; red lines denote 99% confidence interval for baseline firing) to a full screen irradiance increment (time 0–5 s) for a representative center:surround unit inhibited by full-field stimulus.

(H) Heatmaps showing firing rate (scale to right) of a representative center:surround unit when presented (time 0–0.25 s) with either white bars against a black background (i) or black bars against a white background (ii) at various elevations.

(I) Pie chart depicting the proportion of single units that display each of the RF types ("FF" denotes full field; n = 27 cells from 11 mice).

(J) Approximate anatomical location of recording sites at which units with each RF type were recorded superimposed upon schematic of the SCN in coronal (above) and sagittal (below) projection. Dotted lines represent boundaries of SCN; 3V, 3rd; C, caudal; D, dorsal; R, rostral; V, ventral.

See also Figure S1.

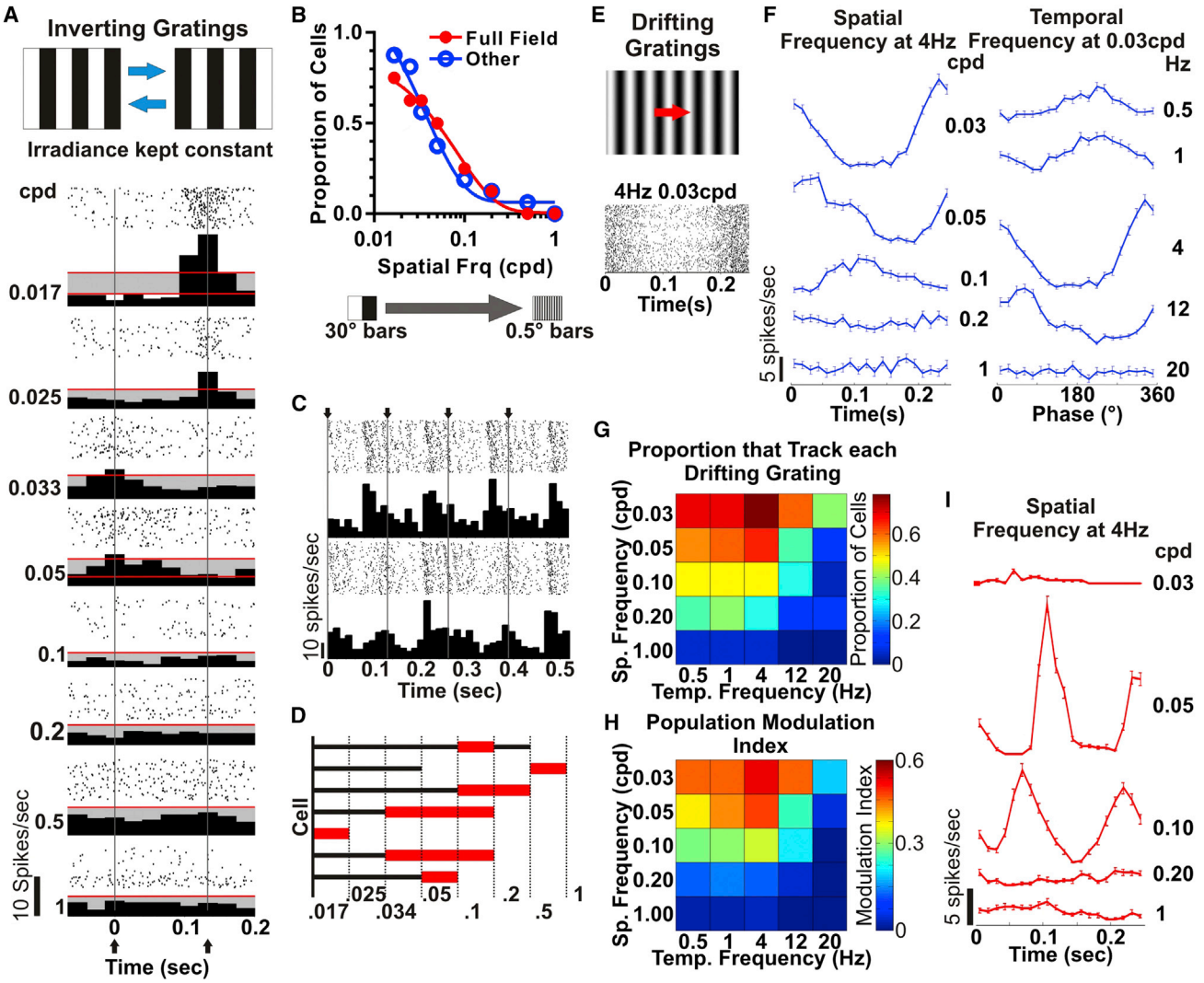

Figure 2. Modulation of SCN Firing by Drifting and Inverting Gratings

(A–D) Single-unit data, n = 24 from six mice. (A) Raster and perievent histogram responses of a representative unit to inverting gratings (~4 Hz; depicted in cartoon form above) as a function of spatial frequency (figures to left in cycles per degree [cpd]) are shown. Red lines indicate ± 3 SDs of mean firing rate across cycle; inversions are at 0 and 0.125 s. (B) Proportion of cells with full-field (n = 8) or "other" (n = 16 either ON center or center:surround) RFs with significant modulations in firing at the grating inversion frequency (spectral power analysis) as a function of spatial frequency is shown. (C) Perievent histograms and rasters over two stimulus cycles (arrows depict inversion times) for two example units exhibiting frequency doubling are shown. (D) The range of spatial frequencies (cpd) over which the seven cells that show frequency doubling responded (black lines) and exhibited frequency doubling (red bar) is shown.

(E) Raster plot for a representative unit under 4-Hz 0.03-cpd stimulus (depicted in cartoon form above).

(F) Firing rate profiles (mean ± SEM 5-min presentation) for a representative unit over a range of spatial (left) and temporal (right) frequencies.

(G) Heatmap (scale to right) of the proportion of cells (n = 23 single units from eight mice) tracking (power at F1 or F2 peak > 4 SDs above the mean) drifting grating at each spatiotemporal frequency.

(H) Heatmap (scale to right) of mean modulation index across the population at different spatiotemporal frequencies (modulation index set to 0 for units without significant response to stimulus).

(I) Firing rate profiles (mean ± SEM 1,200 repeats) over a range of spatial frequencies for a unit with spatial band pass behavior.

See also Figures S1 and S2.

frequencies (spectral power analysis; see STAR Methods). More surprisingly, so did many (6/8) units with a full field response. The ability of SCN units with full field RFs to track these gratings could arise from non-linear summation of input across their RF. Consistent with this interpretation, we found several examples of frequency doubling in grating responses (see STAR Methods; Figure 2C). Such frequency doubling was most prevalent at higher spatial frequencies (Figure 2D), indicating that it arose from non-linear spatial summation as opposed to excitatory responses to both radiance increments and decrements (ON-OFF responses).

The representative examples in Figure 2 indicate that grating inversions could have a large impact on firing rates. To express this more quantitatively, we calculated a modulation index

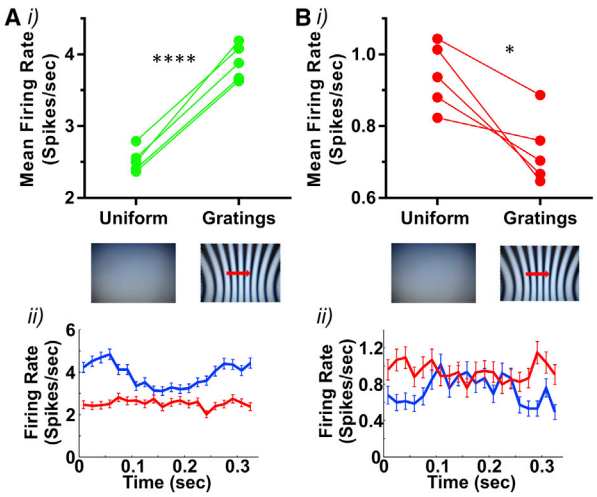

Figure 3. The Effect of Spatial Patterns on Time-Averaged Firing Rate

(A) Response of a representative unit showing higher firing under drifting grating (0.10 cpd; 3 Hz) than a full-field gray stimulus of equivalent irradiance (9×10^{14} photons.cm^{-2}.s^{-1}). (i) Mean firing rate over five sequential presentations of gray and grating stimuli (5 min each; paired t test; $p < 0.0001$) is shown. (ii) Firing rate profile (mean ± SEM) across a cycle of the grating (blue) or an equivalent time window under gray screen (red) is shown.

(B) As in (A) but for a unit showing lower firing under drifting grating (paired t test; $p < 0.05$).

(C) Percentage change in multiunit firing rate (n = 122 recording sites for five mice) under grating compared to uniform gray conditions ($100\% \times (FR_{Grating} - FR_{Uniform})/FR_{Uniform}$; median and interquartile range shown in red).

See also Figures S1 and S3.

([peak − trough]/[peak + trough]) for the firing rate of each unit. At the lowest grating frequency, the mean ± SEM modulation index was 0.95 ± 0.02 (n = 19), indicating that the modulation in firing encompassed nearly the whole range of activity available to the neuron under these conditions.

To determine the types of spatial stimuli to which SCN cells are most responsive, we next set out to examine their spatiotemporal tuning characteristics by applying drifting sinusoidal gratings (contrast ratio 1:600) at a range of spatial (0.03–1 cpd) and temporal (0.5–20 Hz) frequencies. Of 36 light-responsive SCN units from eight mice, 23 showed a significant response to at least one of the gratings presented (spectral power analysis; see STAR Methods). In most cases, these cells responded to a wide range of spatiotemporal frequencies (Figure 2F). The modulation index at the preferred spatiotemporal frequency for each cell varied from 0.25 to 1.00 (0.76 ± 0.05 mean ± SEM). More than half of the units showed a significant modulation at all temporal frequencies ≤12Hz (Figure 2G). The number of units responding peaked at 4 Hz, and this was also the frequency at which response amplitude was highest (Figure 2H).

At the appropriate temporal frequency, responses were most commonly observed for the lowest spatial frequency (0.03 cpd; Figure 2G). However, we did find cells with strong preference for higher spatial frequencies, as predicted for units with strong center:surround antagonism, and indicative of spatial band pass behavior (Figure 2I). Although response amplitude fell away at higher spatial frequencies for all cells, there were clear examples of units that could track 0.2-cpd gratings (Figure S2), indicating that some SCN units have spatial acuity comparable with that reported for more conventional visual structures in this species [17, 18].

Impact of Spatial Patterns on Maintained Activity

The response to drifting and inverting gratings reveals that spatial patterns strongly modulate SCN firing at a fine temporal scale. Previous studies have shown that diffuse illumination increases the maintained firing rate of the SCN [1, 2, 4, 8]. We next asked whether these two modes of SCN activity interact by investigating whether the appearance of spatial patterns altered the time-averaged firing of SCN neurons. Mice were presented with interleaved 5-min epochs of a spatially uniform (gray screen) stimulus or drifting gratings (0.1 cpd; 3 Hz) matched for irradiance (five repeats). Paired t test comparisons revealed a statistically significant ($p < 0.05$; across five repeats) difference in time-averaged firing between the two conditions in 50% (16/32) of light-responsive single units (Figures 3A and 3B). Of these, 81% (13/16 units) showed higher firing rate under gratings (median difference: 0.78 spikes/s [44% increase]; interquartile range: 0.2–2.4 spikes/s [8%–144% increase]) and the remainder showed lower firing under gratings (median difference: 2.7 spikes/s or 23% decrease). The inclusion of spatiotemporal contrast thus disrupts the relationship between irradiance and maintained firing in ~50% of SCN units.

To gain an impression of the impact of this effect on global SCN activity, we analyzed multiunit activity recorded at 122 sites from the five mice. The outcome of this analysis was broadly equivalent to that of single units. Thus, whereas at some sites firing rate was substantially higher under gratings, in many cases, there was little effect (Figure 3C). Overall, there was a small, but statistically significant, increase in maintained activity under drifting gratings (median = 7.8% interquartile range [−2.5%–22%]; n = 122; Wilcoxon test; $p < 0.0001$).

Circadian Phase Resetting in the Presence of Spatial Patterns

Spatial patterns thus substantially alter the fine timing of spikes across the majority of SCN neurons whereas their impact on maintained activity is more variable, with many single units showing little change in this parameter. As maintained activity has previously been reported to track irradiance, we might predict that circadian phase resetting in the SCN should be rather unaffected by spatial patterns. To test this, we measured phase shifts in circadian locomotor activity rhythms of mice free running in constant darkness and exposed for 15 min to an array of LCD screens presenting either spatially uniform (gray screen) or structured (grating) stimuli (Figures 4A and 4B). We first used this apparatus to construct irradiance response curves for uniform gray and drifting sinusoidal gratings (4 Hz; 0.03 cpd). The relationship between phase shift magnitude and stimulus irradiance across the two conditions could be fit with a single sigmoidal

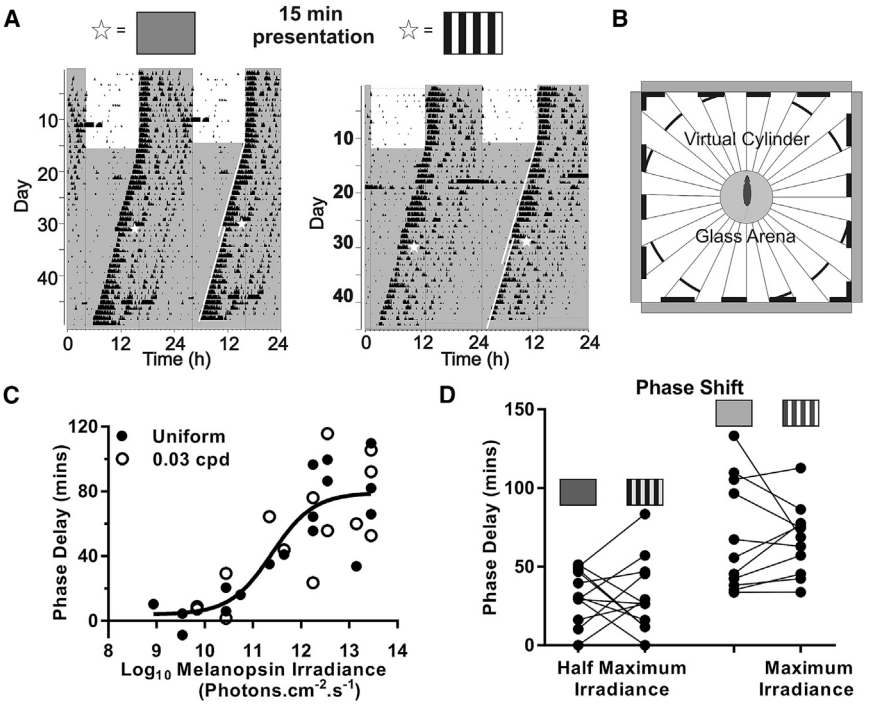

Figure 4. The Effect of Spatially Patterned Stimuli on Phase Shifting

(A) Double-plotted actograms and phase shift of the same mouse to different light pulse stimuli. Mice were pulsed at CT 16 with either a grating- or an irradiance-matched spatially uniform gray screen.

(B) Stimulus set up for the light pulse. Mice were placed in a glass area surrounded by four monitors.

(C) Irradiance response curve for both spatially uniform stimuli (filled circles) and drifting sinusoidal gratings (0.03 cpd; 4 Hz; open circles). Maximum irradiance was 8.7×10^{13} total photons.cm^{-2}.s^{-1}. No significance was observed between curves (linear $p = 0.89$; sigmoidal $p = 0.99$; graph plotted with sigmoidal function of pooled data).

(D) Paired t test for intra-individual responses between a static square wave grating (0.03 cpd) and a uniform stimuli at both the irradiance that produced the half-maximal (8.6×10^{11} total photons.cm^{-2}.s^{-1}) and maximal (6.4×10^{13} total photons.cm^{-2}.s^{-1}) response. No difference between the spatial patterned stimuli and the uniform stimuli was detected at either irradiance (half maximum: $p = 1.00$; maximal: $p = 0.78$).

function (Figure 4C; F-test; $p = 0.99$), indicating that phase resetting was equivalent under uniform and structured stimuli across this irradiance range. As a further test of this conclusion, we used these data to identify irradiances driving maximal and half-maximal phase shifts and presented spatially uniform and square wave grating (to maximize local contrast) stimuli to 12 mice at these irradiances. The inclusion of gratings did not significantly impact phase shift magnitude at either irradiance (paired t test; $p = 1.00$ and $p = 0.78$, respectively; Figure 4D).

DISCUSSION

The accepted function of the retinohypothalamic tract (RHT) is to bring information about background light intensity (irradiance) to the SCN circadian clock. Accordingly, there has been little investigation of the significance of the spatial distribution of light across the visual scene on SCN activity. Yet spatial patterns are an unavoidable feature of our visual experience, and entrainment in mammals originates in the eye, an organ specifically designed to retain spatial information. We find here that the SCN is, in fact, very responsive to spatial patterns. Indeed, an unbiased assessment would identify spatial distribution as being at least as large an influence on SCN firing as irradiance.

Our data reveal that >75% of light-responsive units track inverting or drifting gratings with high-amplitude variations in firing rate. This behavior is, in some cases, found in neurons whose large RFs make them also optimized for detecting irradiance. But such full field units comprise a relatively small fraction of visually responsive SCN neurons. Most units have RFs whose characteristics are optimized for responding to spatial patterns. Thus, the most frequently encountered units have center:surround antagonism, with ON centers as small as could be achieved given the dendritic field of the afferent ganglion cells and large inhibitory surrounds that reduce their sensitivity to diffuse changes in irradiance. This characteristic is absent from the M1 ipRGCs that dominate the SCN projection [7, 19–21]. It is possible that it is present in some other ganglion cell innervating the SCN [21], although to our knowledge such extensive inhibitory surrounds have not been reported for any mouse ganglion cell type. We therefore think it is more likely that the center:surround behavior arises within the brain, either within the SCN itself (Figure S3) or perhaps from connections with other visual centers [22]. Whatever its origin, the appearance of center:surround antagonism produces cells especially responsive to spatial patterns. The same is true of SCN units lacking the inhibitory surround but with spatially constrained ON centers. Thus, where RFs for such units were large enough to require input from multiple RGCs, they were still continuous. This indicates input from neighboring retinal locations and implies an order to the retinal projection that maintains spatial information.

What can we infer about SCN activity under natural viewing conditions from the findings of this study? We first consider the situation in which a subject views a static scene that includes substantial spatial contrast (patterns). Thanks to head, eye, and body movements, the projection of this scene on the retina is never stationary for long. As a result, the retina experiences a moving pattern. The firing of ON center and center:surround units will respond to this event as regions of high and low radiance move across RF centers. Our recordings with drifting and inverting gratings indicate that many full-field units will too thanks to non-linear summation across their RF. Our data thus predict that, under natural conditions, the spatial distribution of light will have a significant impact on the temporal profile of firing of individual SCN units. This modulation is produced by shifts in the image projected onto the retina (associated with changes in

gaze). The degree of modulation in firing will be determined by the amplitude:frequency distribution of head and eye movements in conjunction with the spatial scale(s) and contrast of patterns within the scene. Movement of objects in the visual scene will provide an additional source of modulation.

Although spatial patterns impact the fine timing of firing in the SCN, they had a relatively minor impact on time-averaged firing. This is important, as it is that latter parameter that has previously been shown to encode irradiance [1, 2, 4, 8], and implies that the SCN multiplexes information about irradiance and spatial patterns in different time domains. The further implication, that the irradiance code is relatively unaffected by differences in spatial contrast, provides an explanation for our finding that the inclusion of spatial patterns did not impact circadian phase resetting. This has direct practical relevance. Light therapy for circadian and circadian-related disorders typically employs light boxes presenting diffuse illumination. However, there is no empirical evidence that diffuse light sources engage the SCN most effectively. Our data suggest that displays capable of presenting visual images (televisions, computer monitors, etc.) to which people have an intrinsic attraction, are at least as effective at engaging the SCN [23].

A final implication of the limited impact of spatial contrast on irradiance responses is that the spatial distribution of light need not be considered when assessing the circadian impact of natural or artificial light environments. However, a caveat to this conclusion is that the variation in radiance available from the visual displays used here is small compared to that encountered in the real world. It therefore remains possible that very high spatial contrast environments (e.g., containing spot light sources) would produce a more substantial change in the irradiance code. An analogous effect has been reported for temporal contrast, in which very brief flashes have been used to hyperexcite ipRGCs or enhance circadian photosensitivity [24–27]. Extreme spatial contrast might also induce such circadian visual illusions.

If the modulations in firing over time induced by the appearance and movement of spatial patterns are not relevant for circadian phase resetting, do they perform any function? The SCN is an important control center for numerous physiological systems [28]. Its outputs are known to provide regulation according to time of day and, indeed, irradiance. Could they also allow these systems to respond to more complex visual features? Our data reveal the SCN's capacity to convey such information and provide an explanation for a recent behavioral study indicating SCN involvement in a spatial vision task [5]. We hope that future work will explore the relevance of this newly appreciated sensory capacity for other systems under the SCN's control.

STAR★METHODS

Detailed methods are provided in the online version of this paper and include the following:

- KEY RESOURCES TABLE
- CONTACT FOR REAGENT AND RESOURCE SHARING
- EXPERIMENTAL MODEL AND SUBJECT DETAILS
  - Animals
  - In vivo electrophysiology
  - Visual displays
  - Visual stimuli
  - Phase Shifting Paradigm
- QUANTIFICATION AND STATISTICAL ANALYSES
  - Spike Sorting
  - Receptive Field Mapping
  - Power spectrum analysis
  - Modulation Index
  - Phase Shifts
  - Statistics
- DATA AND SOFTWARE AVAILABILITY

SUPPLEMENTAL INFORMATION

Supplemental Information includes three figures and can be found with this article online at http://dx.doi.org/10.1016/j.cub.2017.04.039.

AUTHOR CONTRIBUTIONS

R.J.L., T.M.B., and J.W.M. conceived and designed the in vivo experiments. J.W.M. conducted the in vivo experiments and performed analysis. A.R.S. and D.B.F. designed and implemented the in silico experiments. The manuscript was written by R.J.L. and J.W.M. with input from all authors.

ACKNOWLEDGMENTS

This work was supported by grants from the Biotechnological and Biological Sciences Research Council (BB/J014478/1), the European Research Council (268970), and the Biomathematics Program at the Army Research Laboratory (W911NF-13-01-0449). We thank Jonathon Wynne, Annette Allen, and Franck Martial for fruitful discussions and technical assistance.

Received: February 24, 2017
Revised: March 27, 2017
Accepted: April 19, 2017
Published: May 18, 2017

REFERENCES

1. Groos, G., and Mason, R. (1978). Maintained discharge of rat suprachiasmatic neurons at different adaptation levels. Neurosci. Lett. *8*, 59–64.
2. Meijer, J.H., Watanabe, K., Schaap, J., Albus, H., and Détári, L. (1998). Light responsiveness of the suprachiasmatic nucleus: long-term multiunit and single-unit recordings in freely moving rats. J. Neurosci. *18*, 9078–9087.
3. Aggelopoulos, N.C., and Meissl, H. (2000). Responses of neurones of the rat suprachiasmatic nucleus to retinal illumination under photopic and scotopic conditions. J. Physiol. *523*, 211–222.
4. Brown, T.M., Wynne, J., Piggins, H.D., and Lucas, R.J. (2011). Multiple hypothalamic cell populations encoding distinct visual information. J. Physiol. *589*, 1173–1194.
5. Yu, Y.-Q., Barry, D.M., Hao, Y., Liu, X.-T., and Chen, Z.-F. (2017). Molecular and neural basis of contagious itch behavior in mice. Science *355*, 1072–1076.
6. Foster, R.G., and Soni, B.G. (1998). Extraretinal photoreceptors and their regulation of temporal physiology. Rev. Reprod. *3*, 145–150.
7. Zhao, X., Stafford, B.K., Godin, A.L., King, W.M., and Wong, K.Y. (2014). Photoresponse diversity among the five types of intrinsically photosensitive retinal ganglion cells. J. Physiol. *592*, 1619–1636.
8. Groos, G.A., and Mason, R. (1980). The visual properties of rat and cat suprachiasmatic neurones. J. Comp. Physiol. *135*, 349–356.
9. Walmsley, L., and Brown, T.M. (2015). Eye-specific visual processing in the mouse suprachiasmatic nuclei. J. Physiol. *593*, 1731–1743.

10. Berson, D.M., Dunn, F.A., and Takao, M. (2002). Phototransduction by retinal ganglion cells that set the circadian clock. Science *295*, 1070–1073.
11. Spitschan, M., Datta, R., Stern, A.M., Brainard, D.H., and Aguirre, G.K. (2016). Human visual cortex responses to rapid cone and melanopsin-directed flicker. J. Neurosci. *36*, 1471–1482.
12. Allen, A.E., Storchi, R., Martial, F.P., Bedford, R., and Lucas, R.J. (2017). Melanopsin contributions to the representation of images in the early visual system. Curr. Biol. *27*, this issue, 1623–1632.
13. Schmidt, T.M., Do, M.T.H., Dacey, D., Lucas, R., Hattar, S., and Matynia, A. (2011). Melanopsin-positive intrinsically photosensitive retinal ganglion cells: from form to function. J. Neurosci. *31*, 16094–16101.
14. Estevez, M.E., Fogerson, P.M., Ilardi, M.C., Borghuis, B.G., Chan, E., Weng, S., Auferkorte, O.N., Demb, J.B., and Berson, D.M. (2012). Form and function of the M4 cell, an intrinsically photosensitive retinal ganglion cell type contributing to geniculocortical vision. J. Neurosci. *32*, 13608–13620.
15. Remtulla, S., and Hallett, P.E. (1985). A schematic eye for the mouse, and comparisons with the rat. Vision Res. *25*, 21–31.
16. Meijer, J.H., Groos, G.A., and Rusak, B. (1986). Luminance coding in a circadian pacemaker: the suprachiasmatic nucleus of the rat and the hamster. Brain Res. *382*, 109–118.
17. Grubb, M.S., and Thompson, I.D. (2003). Quantitative characterization of visual response properties in the mouse dorsal lateral geniculate nucleus. J. Neurophysiol. *90*, 3594–3607.
18. Niell, C.M., and Stryker, M.P. (2008). Highly selective receptive fields in mouse visual cortex. J. Neurosci. *28*, 7520–7536.
19. Güler, A.D., Ecker, J.L., Lall, G.S., Haq, S., Altimus, C.M., Liao, H.-W., Barnard, A.R., Cahill, H., Badea, T.C., Zhao, H., et al. (2008). Melanopsin cells are the principal conduits for rod-cone input to non-image-forming vision. Nature *453*, 102–105.
20. Hatori, M., Le, H., Vollmers, C., Keding, S.R., Tanaka, N., Buch, T., Waisman, A., Schmedt, C., Jegla, T., and Panda, S. (2008). Inducible ablation of melanopsin-expressing retinal ganglion cells reveals their central role in non-image forming visual responses. PLoS ONE *3*, e2451.
21. Baver, S.B., Pickard, G.E., Sollars, P.J., and Pickard, G.E. (2008). Two types of melanopsin retinal ganglion cell differentially innervate the hypothalamic suprachiasmatic nucleus and the olivary pretectal nucleus. Eur. J. Neurosci. *27*, 1763–1770.
22. Hanna, L., Walmsley, L., Pienaar, A., Howarth, M., and Brown, T.M. (2017). Geniculohypothalamic GABAergic projections gate suprachiasmatic nucleus responses to retinal input. J. Physiol. Published online February 20, 2017. http://dx.doi.org/10.1113/JP273850.
23. Chang, A.M., Aeschbach, D., Duffy, J.F., and Czeisler, C.A. (2015). Evening use of light-emitting eReaders negatively affects sleep, circadian timing, and next-morning alertness. Proc. Natl. Acad. Sci. USA *112*, 1232–1237.
24. Vartanian, G.V., Zhao, X., and Wong, K.Y. (2015). Using flickering light to enhance nonimage-forming visual stimulation in humans. Invest. Opthalmol. Vis. Sci. *56*, 4680–4688.
25. Vidal, L., and Morin, L.P. (2007). Absence of normal photic integration in the circadian visual system: response to millisecond light flashes. J. Neurosci. *27*, 3375–3382.
26. Zeitzer, J.M., Ruby, N.F., Fisicaro, R.A., and Heller, H.C. (2011). Response of the human circadian system to millisecond flashes of light. PLoS One *6*, e22078.
27. Zeitzer, J.M., Fisicaro, R.A., Ruby, N.F., and Heller, H.C. (2014). Millisecond flashes of light phase delay the human circadian clock during sleep. J. Biol. Rhythms *29*, 370–376.
28. Kalsbeek, A., Yi, C.X., Cailotto, C., la Fleur, S.E., Fliers, E., and Buijs, R.M. (2011). Mammalian clock output mechanisms. Essays Biochem. *49*, 137–151.
29. Allen, A.E., Storchi, R., Martial, F.P., Petersen, R.S., Montemurro, M.A., Brown, T.M., and Lucas, R.J. (2014). Melanopsin-driven light adaptation in mouse vision. Curr. Biol. *24*, 2481–2490.
30. Smallwood, P.M., Olveczky, B.P., Williams, G.L., Jacobs, G.H., Reese, B.E., Meister, M., and Nathans, J. (2003). Genetically engineered mice with an additional class of cone photoreceptors: implications for the evolution of color vision. Proc. Natl. Acad. Sci. USA *100*, 11706–11711.
31. Durand, S., Iyer, R., Mizuseki, K., de Vries, S., Mihalas, S., and Reid, R.C. (2016). A comparison of visual response properties in the lateral geniculate nucleus and primary visual cortex of awake and anesthetized mice. J. Neurosci. *36*, 12144–12156.
32. Lall, G.S., Revell, V.L., Momiji, H., Al Enezi, J., Altimus, C.M., Güler, A.D., Aguilar, C., Cameron, M.A., Allender, S., Hankins, M.W., and Lucas, R.J. (2010). Distinct contributions of rod, cone, and melanopsin photoreceptors to encoding irradiance. Neuron *66*, 417–428.
33. Brainard, D.H. (1997). The psychophysics toolbox. Spat. Vis. *10*, 433–436.
34. Pelli, D.G. (1997). The VideoToolbox software for visual psychophysics: transforming numbers into movies. Spat. Vis. *10*, 437–442.
35. Howarth, M., Walmsley, L., and Brown, T.M. (2014). Binocular integration in the mouse lateral geniculate nuclei. Curr. Biol. *24*, 1241–1247.

STAR★METHODS

KEY RESOURCES TABLE

REAGENT or RESOURCE	SOURCE	IDENTIFIER
Chemicals, Peptides, and Recombinant Proteins		
Urethane	Sigma-Aldrich	Cat# U2500
DiI	Thermo Fisher	Cat# V22885
Experimental Models: Organisms/Strains		
Mouse: C57BL/6	Envigo	Code: 057
Mouse: *Opn1mw*^{R}	Dr. Jeremy Nathans, Johns Hopkins University [24]	
Software and Algorithms		
The Chronobiology Kit: KitCollect, KitMonitor, KitAnalyzer	Stanford Software Systems	https://query.com/chronokit/
Recorder64	Plexon	http://file.yizimg.com/415758/2013051615482882.pdf
PlexUtil [ver 2.1.2]	Plexon	http://www.plexon.com/products/plexutil
OfflineSorter [ver 3.]	Plexon	http://www.plexon.com/products/offline-sorter
NeuroExplorer [ver 4.]	NeuroExplorer	http://www.neuroexplorer.com/downloadspage/
MATLAB R2013	MathWorks	https://uk.mathworks.com/products/matlab.html
Psychophysics Toolbox	http://psychtoolbox.org/	http://psychtoolbox.org/
GraphPad Prism 6	GraphPad	http://www.graphpad.com/
Other		
LCD Monitor	ViewSonic	VA2037-LED
LCD Monitor	DynaScan	DS46LO4
Custom projector system	Prof. Rob Lucas, University of Manchester [29]	

CONTACT FOR REAGENT AND RESOURCE SHARING

Further information and requests for resources and reagents should be directed to and will be fulfilled by the Lead Contact, Rob Lucas (Robert.Lucas@manchester.ac.uk).

EXPERIMENTAL MODEL AND SUBJECT DETAILS

Animals

All experiments used adult (> 8 weeks) male mice from a C57BL/6 background strain (Envigo, Bicester, UK). Animals were group housed under a 12:12 light/dark cycle, with food and water available ad libitum. All experiments received institutional ethics committee approval and in accordance with UK Animals (Scientific Procedures) Act 1986, and European Directive 2010/63/EU.

In vivo electrophysiology

In vivo electrophysiology was performed on mice aged between 8 to 17 weeks old. The majority of experiments employed wild-type C57BL/6 mice (Envigo, Bicester, UK) although *Opn1mw*^{R} mice [30] were used for the inverting grating experiments. The phenotype (enhanced sensitivity to red light) of these *Opn1mw*^{R} is not expected to alter their response to spatial stimuli. Mice were housed on an inverted light dark cycle so that electrophysiological recordings were performed during the early subjective night when the response to light is greatest [4] and to minimize the possible circadian variation of SCN cell's response to light [3].

Behaviour

Wild-type C57BL/6 mice (Envigo, Bicester, UK) were individually housed in running wheel cages. Mice were housed under a 6 week light schedule consisting of 2 weeks of a 12:12 light/dark cycle, followed by continuous darkness (DD) for 4 weeks.

METHOD DETAILS

In vivo electrophysiology

Extracellular recordings were made under urethane anaesthetisia (i.p.;1.5g/kg) on a homeothermic heat mat (Harvard Apparatus, UK) as previously described [4]. Anaesthesia is expected to reduce the amplitude of visual responses but not to impact relative sensitivity

to different visual features [31]. Briefly, 4x8 recording electrode arrays (Buzsaki32L electrodes (NeuroNexus Technologies, MI)) were introduced to the SCN based upon stereotaxic coordinates. Activity was recorded using Recorder64 (Plexon, TX), signals amplified by a 20x gain AC-coupled headstage (Plexon, TX) followed by pre-amplifier conditioning providing a total gain of 3500x; filtered with Butterworth 250Hz high-pass filter. Signals passing a 35mV threshold were timestamped and their waveforms digitized at a rate of 40 KHz. The raw signal was also digitalized. All data were stored for offline analysis. Dipping the electrode in fluorescent dye (Cell Tracker CM-DiI; Invitrogen, UK) prior to insertion allowed the electrode track to be visualized in coronal sections of fixed brain (4% PFA).

Visual displays

Spectral irradiances (350-800nm) for visual displays were recorded using a spectroradiometer (Bentham Instruments Ltd, UK) and effective photon flux for each mouse photopigment calculated as previously described [29]. Behavioral experiments employed a square arena formed by 4 x RGB monitors (Viewsonic; VA2037-LED). In electrophysiological recordings stimuli were applied to the eye contralateral to the electrode insertion site (ipsilateral eye covered) with an RGB monitor (DS46LO4; Dynascan), except for the inverting gratings which were applied using a custom made source consisted of four independently controlled LEDs (λ_{max} 405, 455, 525, and 630 nm; Phlatlight PT-120 Series, Luminus, Sunnyvale, CA, USA), presented through a digital mirror device projector (DLP LightCommander; Texas Instruments Inc, Dallas, TX, USA). At full screen white the Dynascan produced: 11.6 (S-cone), 14.9 (M/L cone) and 14.8 (Rod and melanopsin) log(effective photons/cm^2/s); and the custom display: 11.9 (S-cone) and 13.3 (M/L cone, rod, melanopsin) log(effective photons/cm^2/s). The photoreceptor contribution to the SCN varies with irradiance [32] and has been shown to affect the SCN response to full field stimuli [3]. Here we have focused on scotopic light levels, where melanopsin is active.

Visual stimuli

The receptive field mapping protocol comprised a series of white bars (width = 6° for horizontal and 8° for vertical bars) against a black background. Bars were presented for 250ms at a single location at a time, separated by 250ms of 'black' screen, in a randomized sequence (10-30 repeats of each position) and covering each axis at 1° resolution. Grating stimuli (corrected for viewing angle) were created and displayed using MATLAB [ver. R2012a] (The MathWorks, Natick, MA, USA) in conjunction with the psychophysics toolbox extensions [33, 34]. Inverting black and white square-wave gratings were presented at 1.85 or 3.76 Hz inverting grating for 50 s followed by the same inverting grating shifted by a quarter of a cycle. Sinusoidal drifting gratings were presented for 5 min at each spatial and temporal frequency. A smaller range of spatial frequencies (1-0.03cpd) was employed for drifting grating stimuli to allow us to trial each at a number of temporal frequencies within a reasonable recording epoch. Order of presentation for spatial frequencies was randomized. Within a given spatial frequency, the temporal frequencies were presented in ascending order. For comparisons of firing rate between gray screen and sinusoidal grating, stimuli were presented for 5 min, interleaved, with the order of presentation randomized.

Phase Shifting Paradigm

Locomotor activity was monitored with a running wheel linked to a data logging system (The Chronobiology Kit, Stanford Software Systems, Santa Cruz, CA). Mice were housed for 2 weeks in a 12:12 light/dark cycle, then transferred to continuous darkness (DD). 12 days later they were placed within cylindrical glass arena (12.8cm diameter) surrounded by 4 RGB monitors (ViewSonic VA2037-LED) forming a 48 × 48 cm square at CT16 (4 hr after activity onset) and exposed to either gray or grating stimuli for 15 min. Sinusoidal and drifting grating stimuli were presented as a virtual drum based upon the estimated viewing angle of the mouse. Irradiance was modulated with neutral density filters (Lee filters)

QUANTIFICATION AND STATISTICAL ANALYSES

Spike Sorting

Spike sorting was performed as previously described [35] using Offline Sorter [ver.3] (Plexon, TX). Briefly, cross-channel artifacts and noise were removed, leaving multiunit data. Raw data was then combined to form 'virtual'-tetrode waveforms using custom made MATLAB scripts and single units extracted using principle component analysis. Data were then analyzed using NeuroExplorer [ver. 4] (Nex Technologies, MA), MATLAB and GraphPad Prism (ver. 6, GraphPad Software). Light responsive units were defined as those in which firing rates (250ms bins) at light onset or offset fell outside the 99% confidence limits of baseline activity in 5 s prior to stimulus.

Receptive Field Mapping

RFs were mapped using bespoke MATLAB scripts. The perievent histogram (bin size: 10 ms; 50ms moving average) was taken for each vertical and horizontal bar and normalized to the preceding 100 ms. The change of firing rate at time of maximum response (t_{max}) was plotted against bar position and fitted by a Gaussian or a difference of Gaussians using GraphPad Prism. The width of the receptive field in each dimension was taken as full width at half maximum ($2\sqrt{(2\ln 2)}\sigma$).

Classification of units as 'ON center', 'center:surround', and 'full field' ON and OFF were as described in Results section. However, it is likely that this method under-estimates the occurrence of 'center:surround' units. Thus, 'full field OFF' units could in fact be 'center:surround' units whose ON center lies outside of the area covered by our display. In support of this interpretation, in a couple

of cases the inhibitory response was attenuated for bars appearing on the edge of the field of view (Figure 1B). Similarly, some 'ON center' units had very low baseline firing making it difficult to determine whether they were refractory to, or inhibited by, bars outside of the RF center.

Power spectrum analysis

Power spectrum analysis was performed using a custom MATLAB script and performed both on the spike times and the shuffled spike times. The 'shuffled' power spectrum was subtracted from the 'original' power spectrum and then normalized to the standard deviation of the new spectrum. The peak power was chosen within 2 bins of both the predicted F1 and F2 frequencies for inverting gratings and 6.5 bins for drifting gratings. The normalized power was averaged over 1000 repeats. F1 or F2 values greater than 3.5 standard deviations above the mean were considered significant for inverting gratings and 4 standard deviations for inverting gratings (accounting for the larger window for peak and increased number of trials). Units with significant oscillations in which the F2 power was greater than F1 power were considered to show frequency doubling.

Modulation Index

Perievent histograms for firing under inverting (26.7ms bins and a 5 bin moving average) or drifting (10 bins/cycle) gratings were used to determine the maximum and minimum instantaneous firing rates. If a cell tracked a spatial frequency at both phases, then the maximum of the two amplitudes was used. Modulations index was set to 0 for units with no significant response in power spectrum analysis.

Phase Shifts

Phase shifts between activity onset on day of pulse predicted from records before versus after the stimulus were the mean of 3 independent estimates made by experienced scorers blind to treatment.

Statistics

Details about standard statistical tests performed using GraphPad Prism are reported in the main text and figure legends.

DATA AND SOFTWARE AVAILABILITY

Raw data and analysis/stimulus code will be provided upon request by the Lead Contact Rob Lucas (Robert.Lucas@manchester.ac.uk).

Current Biology, Volume *27*

Supplemental Information

Responses to Spatial Contrast in the Mouse Suprachiasmatic Nuclei

Joshua W. Mouland, Adam R. Stinchcombe, Daniel B. Forger, Timothy M. Brown, and Robert J. Lucas

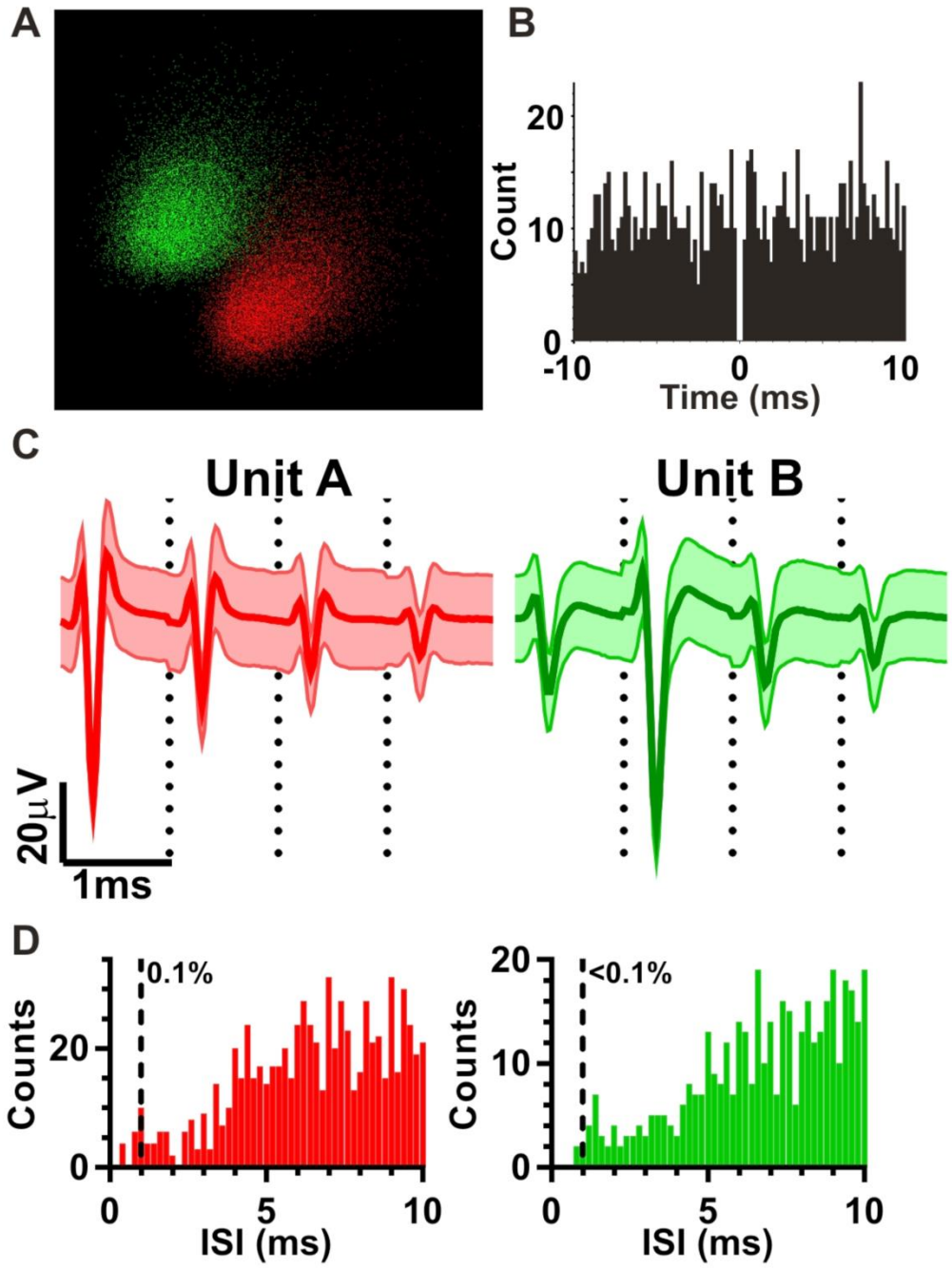

Figure S1: Spike sorting Validation. Related to Figures 1-3. A-D. Show two single units that were located on the same tetrode (unit A in red and unit B in green). **A.** The two units separated using principle component analysis and waveform parameters. Here peak to trough amplitude on electrode site one and two respectively. **B.** Crosscorrelogram of unit A vs unit B (bin size =0.2 ms). **C.** The tetrode waveform for each unit (mean±s.d.). Each tetrode waveform is comprised of the waveform at a given epoch across four electrode sites. The dotted line denotes the start of the epoch for each electrode. **D.** Interspike interval for each unit (0.2 ms bins). The dashed black line denotes the percentage of spikes that fall within 1ms of another spike.

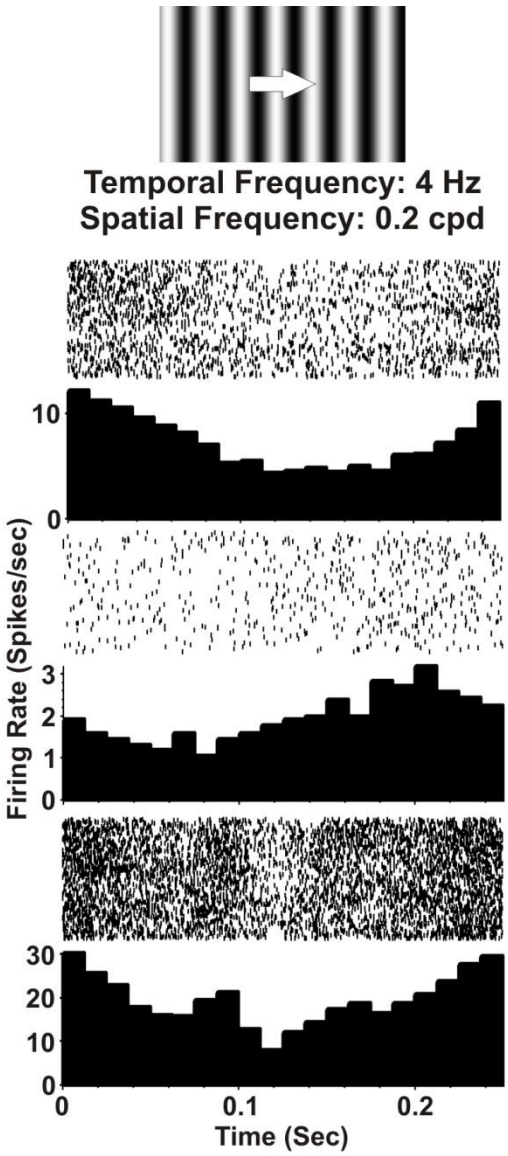

Figure S2: Single units tracking drifting gratings at 0.2cpd. Related to Figure 2. Perievent histogram (above) and raster plots (below) of spike firing (12.5 ms bins) from three single units that showed significant modulation (as determined by spectral power analysis) by a drifting sinusoidal grating at 0.2cpd (1200 repeats at 4Hz).

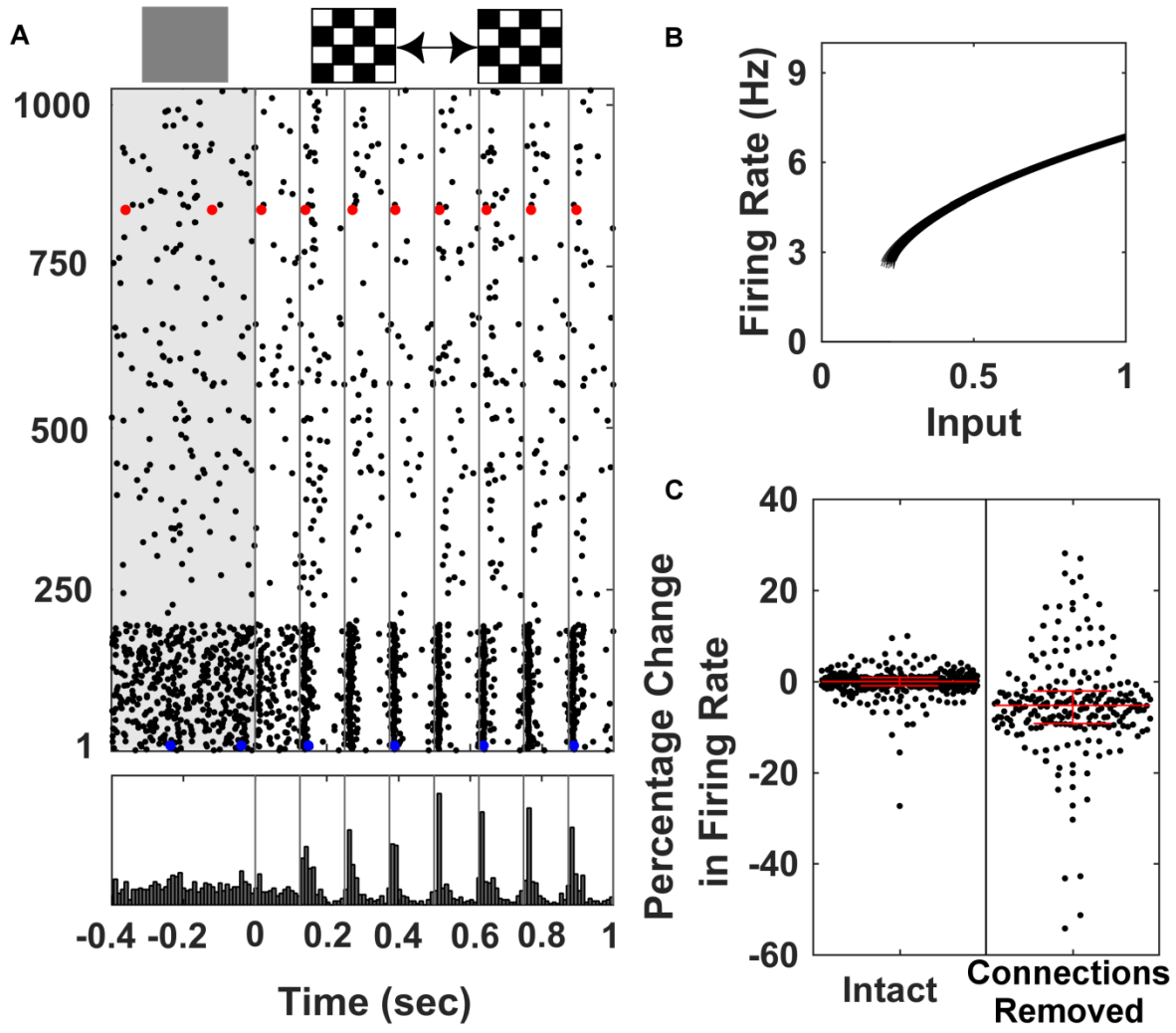

Figure S3: A simulation of the electrical activity of the SCN. Related to Figure 3. The membrane voltage of each of 1024 neurones evolve according to a conductance-based model that incorporates sodium, potassium, and calcium currents and has been fit previously to extensive electrophysiology experiments[S1-4]. Each SCN neurone receives synaptic input from other SCN neurons, while a subset of the SCN neurons receive input from a 14 by 14 array of ipRGCs whose receptive fields tile a detail of the visual scene. The connectivity within the SCN and from the retina to the SCN has been selected as to reproduce the range and proportions of the spatial RFs described in this manuscript. **A**. Raster plots of activity (dots represent spikes) over 0.4 second uniform illumination (shaded grey) followed by 1 sec exposure to a 4Hz inverting 14 by 14 chequerboard stimulus. Each stimulus inversion is denoted with a grey vertical line. Below the raster is a histogram of the spike times for the neurones with a bin width of 10ms. Note the widespread 4Hz periodicity in firing (the neurone with blue dots for example) and in some cases frequency doubling (the neurone with red dots for example) that has been observed experimentally. The spatially patterned input affects the timing of spikes for many neurones. **B.** The input-output relation of a single model SCN neurone. The steady firing rate of a model neurone is plotted as a function of constant input for each circadian time at which

experimental data was collected. They show a uniform input threshold to generate firing and a saturating of the firing rate for large inputs. According to this input-output relation, we expect that an individual neurone could have either a higher or lower firing rate for patterned input over uniform illumination depending on its retinal and SCN network inputs. **C.** Distribution of changes in firing rates of 381 (Intact) and 222 (Connections Removed) simulated spiking SCN neurones from a uniform grey condition to a 4Hz inverting 14 by 14 chequerboard stimulus (100% x (FRinverting chequerboard - FRUniform)/FRUniform; median and interquartile range shown in red). Both increases and decreases in the firing rates are observed, matching experimental data in Figure 3C. The network within the SCN acts to attenuate the overall impact of contrast since after removing these connections the SCN neurones show a greater spread in firing rate in response to the patterned stimulus.

Supplemental References

[S1] Diekman, C.O., and Forger, D.B. (2009). Clustering Predicted by an Electrophysiological Model of the Suprachiasmatic Nucleus. J. Biol. Rhythms *24*, 322–333.

[S2] Diekman, C.O., Belle, M.D.C., Irwin, R.P., Allen, C.N., Piggins, H.D., and Forger, D.B. (2013). Causes and Consequences of Hyperexcitation in Central Clock Neurons. PLoS Comput. Biol. *9*, e1003196.

[S3] DeWoskin, D., Myung, J., Belle, M.D.C., Piggins, H.D., Takumi, T., and Forger, D.B. (2015). Distinct roles for GABA across multiple timescales in mammalian circadian timekeeping. Proc. Natl. Acad. Sci. *112*, E3911–E3919. Available at: http://www.pnas.org/lookup/doi/10.1073/pnas.1420753112.

[S4] Dewoskin, D., Geng, W., Stinchcombe, A.R., and Forger, D.B. (2014). It is not the parts , but how they interact that determines the behaviour of circadian rhythms across scales and organisms. Interface Focus *4*, 20130076.